Aerodynamics of Slender Rolling Wings at Incidence in Separated Flow

M. J. Cohen* and D. Nimri†
Technion-Israel Institute of Technology, Haifa, Israel

A solution to the problem of slender wings in roll about the wind axis and at angle of attack is presented. The basic approach used is a variation of that of Brown and Michael interpreted to take into account the antisymmetrical component in the resultant flow. A pressure distribution function is derived and plotted in a representative range of the key parameters, $(p,\bar{\alpha},\bar{s}_0)$ and a general expression for the evaluation of the damping contribution in roll caused by leading-edge separation in slender wings is given. The method is applied here for the evaluation of the roll damping moment and pitch coupling of a basic delta-wing, but the pressure distribution function is given in generalized form. This should enable the flow characteristics on more general rolling configurations to be reliably assessed within the limitation of the model adopted.

Nomenclature

$O_0x_0y_0z_0$ = body-fixed axes, originating at wing apex; O_0x_0 along the wing root-chord
$OXYZ$ = space-fixed axes, with OX, the roll axis of the wing in the direction of U and OY parallel to O_0y_0, at any given time t
p = rate of roll of the wing about the wind axis OX
Z-plane = plane $Z=y+iz$, normal to the wing plane at a distance x_0 from the apex O_0, the cross-flow plane
ξ-plane = transformed plane, $\xi=\eta+i\zeta$
c_R = wing root-chord
s = semispan of the trace of the wing in the Z-plane
s_0 = semispan of the wing in the plane $X=0$, at a distance $x_0=x_{00}$ from the apex O_0
s_B = semispan of the wing at the trailing-edge, i.e., at $x_0=c$
$\bar{s}_0$ = nondimensional semispan, $\bar{s}_0=s_0/s$
Γ_i = strength of the detached vortices in the cross-flow plane, $i=1,2$
Z_i = vector position of the detached vortices in the Z-plane $Z_i=y_i+iz_i=|Z_i|e^{i\alpha i}, i=1,2$
$\bar{s}_{0B}$ $=s_0/s_B$
$\bar{p}_0$ $=ps_0/U\epsilon$
ξ_i = vector position of the detached vortices in the ξ-plane $\xi_i=\eta_i+i\zeta_i=\rho_i e^{i\beta i}, i=1,2$
$\gamma(y)$ = strength of the vorticity distribution along trace of wing in the Z-plane
θ = polar angle defined by, $y=s\cos\theta$
U = stream velocity parallel to the plane of symmetry of the wing and at angle-of-attack α to the wing chord
ϵ = half-apex angle of delta-wing $[\epsilon=(s_B/c_R)]$, or local slope of leading edge to stream direction, i.e., ds/dx
$\bar{\alpha}$ = nondimensional angle of attack of the wing i.e., $\bar{\alpha}=\alpha/\epsilon$
$\bar{p}$ $=ps/U\epsilon$ with, $\bar{p}_B=ps_B/U\epsilon$
$\bar{\Gamma}_i$ $=\Gamma_i/2\pi Us\epsilon$, $i=1,2$
$(v_i+iw_i)_-$ = velocity vector residue, at vortex singularity, at $Z=Z_i$, $i=1,2$
u,v,w = perturbation velocity components along Ox, Oy, Oz
C_ℓ $=L/\rho U^2Ss_B$, nondimensional damping in roll coefficient
C_m $=M/\frac{1}{2}\rho U^2Sc_R$, nondimensional pitch coupling due to roll
C_p $=-2u/U-v^2-w^2/U^2+\alpha^2$, pressure coefficient on the wing
ϕ = perturbation velocity potential
ψ = stream function in Z-plane

I. Introduction

A SLENDER wing rolling at a slow rate and at zero angle of attack will experience a hydrodynamic resistance to this roll which is measured by the damping in roll derivative C_{ℓ_p}. This derivative can be assessed quite easily either macroscopically[1-4] or microscopically[5,6] and gives a good measure of the linear damping experienced by a slowly rolling wing. At high rates of roll and at angle of attack, however, separation takes place along the leading edges with a pair of vortex sheets detaching from the rotating edges. These vortex sheets roll up into spiral cornets forming cores of high vorticity concentration at some distance from the leading edges. The resultant flow is not conical, and one can expect an additional basic parameter determining the rolling contribution to be ps_B/U, or, more conveniently, $ps_B/U\epsilon$ in addition to the familiar parameter α/ϵ which introduces the incidence element. It will also be shown that another parameter s_0/s_B, which brings in the position of the roll axis along the wing chord, plays an important part, as could be expected, in determining the character of the flow.

The approach used here is similar to that of Brown and Michael[7] in the sense that apart from the requirement of smooth outflow from the leading edges, the main physical constraint is that imposed on a simplified vortex system consisting of a pair of concentrated vortices joined to the leading edges by cuts across which there exist velocity potential discontinuities. The physical image of these cuts is the trace of the vortex sheets feeding the concentrated vortices and generated along the lengths of the leading edges by the shearing action of the rotating wing on the ambient fluid. This model leads to a statement of the problem in a crossflow plane, the Z-plane, whose geometric and dynamic elements are illustrated in Figs. 1 and 2. This basic model has already been used by Hanin and Mishne[8] to provide a solution, partly numerical, of the particular problem of the rolling slender

Received June 3, 1975; revision received January 14, 1976. The authors wish to thank A. Rosenbaum for her kind and expert handling of the typing of this paper.

Index category: Aircraft Aerodynamics (including Component Aerodynamics).

*Associate Professor, Department of Aeronautical Engineering. Associate Member AIAA.

†Project Engineer, Research & Development Foundation, Department of Aeronautical Engineering.

wing at zero angle of attack. Their procedure is not followed, however, in the more general and complex problem examined here. A solution is obtained, based on suitable assumptions regarding the local rate of development of the concentrated vortices, which enables the local character of the flow to be obtained "independently" of that in neighboring sections. These assumptions were tested against the partly numerical solution of Hanin and Mishne[8] for the $\bar{\alpha}=0$ case, and the agreement was found to be very good. Thus, the approach used keeps close to a theoretical framework suitably helped by acceptable modeling. In this it differs from the intuitive model suggested by Polhamus,[9] which in many cases gives useful practical results. Boyden[10] has applied Polhamus' model to assess the damping in roll of specific slender configurations in detached flow, and his results together with experimental data[11] will be compared with some of the more general results presented in this paper.

II. Analysis

It is easy to show that the relevant complex potential in the Z-plane for a rotating two-dimensional plate at angle of attack α is

$$W_1(Z) = -\frac{ip}{4}(Z-(Z^2-s^2)^{1/2})^2 - i\alpha U(Z^2-s^2)^{1/2} \tag{1}$$

for unseparated flow, where s is the local semispan of the cut. Using the transformation

$$\xi = (Z+(Z^2-s^2)^{1/2})/2 \tag{2}$$

one can transform the flow in the Z-plane into that in a ξ-plane, wherein the cut in the Z-plane transforms into a circular trace of radius $s/2$. In particular, the flow of Eq. (1), corresponding to the unseparated flow round the rotating plate, becomes in the ξ-plane

$$W_1(\xi) = -\frac{ips^2}{4\xi^2} - \frac{i\alpha U}{2}\left(\xi - \frac{1}{\xi}\right) \tag{3}$$

where

$$\bar{\xi} = \frac{2\xi}{2} = \frac{2\rho e^{i\beta}}{s} = \bar{\rho}e^{i\beta}$$

The simplified vortex system associated with separated flow can quite simply be inserted in the ξ-plane (Fig. 3) by means of the additional potential function $W_2(\xi)$, where

$$W_2(\xi) = \frac{i\Gamma_1}{2\pi}\log(\xi-\rho_1 e^{i\beta_1}) + \frac{i\Gamma_2}{2\pi}\log(\xi-\rho_2 e^{i\beta_2})$$
$$-\frac{i\Gamma_1}{2\pi}\log\left(\xi-\frac{s^2e^{i\beta_1}}{4\rho_1}\right) - \frac{i\Gamma_2}{2\pi}\log\left(\xi-\frac{s^2e^{i\beta_2}}{4\rho_2}\right) \tag{4}$$

The complex potential function

$$W(\xi) = W_1(\xi) + W_2(\xi) \tag{5}$$

now satisfies all the geometric and dynamic boundary conditions but with Γ_i, ρ_i, and β_i, $i=1,2$, so far undetermined. These will be determined from physical considerations, including that of "smooth outflow" at the edges in the following paragraph.

Determination of Γ_i, ρ_i, and β_i

The complex potential of Eq. (1) contributes the velocity q

$$q = \lim_{\substack{\theta\to 0 \\ Z\to s}}\left\{\frac{1}{2}ps\left(\frac{1}{\sin\theta}-2\sin\theta\right)\cdot\frac{dZ}{d\xi}\right\} + 2\alpha U \tag{6}$$

in the ξ-plane, at points corresponding to $Z=\pm s$, i.e., at $\xi=\pm s/2$. Since

$$\frac{dZ}{d\xi} = \frac{2(Z^2-s^2)^{1/2}}{Z+(Z^2-s^2)^{1/2}}$$

the limit of Eq. (6) yields

$$\xi = +\frac{s}{2} \qquad q = -ips + 2\alpha iU$$

$$\xi = -\frac{s}{2} \qquad q = +ips + 2\alpha iU$$

In order to ensure smooth outflow at the trace edges in the Z-plane, one enforces the condition that the velocity contribution, at $\xi=\pm(s/2)$, of the flow $W_2(\xi)$, to be: $\pm ips - 2\alpha iU$, i.e.,

$$\left(\frac{dW_2}{d\xi}\right)_{\xi\to\pm(s/2)} = \mp ips + 2i\alpha U$$

Performing the differentiation and limiting processes yields the first two relations between Γ_i, ρ_i, and β_i, $i=1,2$.

$$\frac{\bar{\Gamma}_1(\bar{\rho}_1^2-1)}{\bar{\rho}_1^2+1-2\cos\beta_1} + \frac{\bar{\Gamma}_2(\bar{\rho}_2^2-1)}{\bar{\rho}_2^2+1+2\cos\beta_2} = \frac{\bar{p}}{2} - \bar{\alpha}$$

$$\frac{\bar{\Gamma}_2(\bar{\rho}_2^2-1)}{\bar{\rho}_2^2+1-2\cos\beta_2} + \frac{\bar{\Gamma}_1(\bar{\rho}_1^2-1)}{\bar{\rho}_1^2+1+2\cos\beta_1} = \frac{\bar{p}}{2} + \bar{\alpha} \tag{7}$$

where

$$\bar{\rho} = \frac{2\rho}{s}, \quad \bar{p} = \frac{ps}{U\epsilon}, \quad \bar{\alpha} = \frac{\alpha}{\epsilon}, \quad \Gamma_i = \frac{\Gamma_i}{2\pi sU\epsilon}$$

Thus for every pair of values of the key nondimensional performance parameters $(\bar{p}, \bar{\alpha})$, Eqs. (7) yield two relations between the six parameters $\bar{\Gamma}_i$, ρ_i, and β_i, $i=1,2$. Four more relations are yielded by the stipulation that the net force vector exerted by the ambient fluid on each of the *combined* systems of feeding vortex layer and concentrated vortex generated by each edge, is zero. A mathematical expression of this condition is:

$$(v_i+iw_i)_- = \epsilon U\{(n_i+1)\bar{Z}_i \mp n_i + i\bar{p}[\bar{Z}_i + i\alpha(\bar{x}_{00}-\bar{x}_0)]\} \tag{8}$$

where $\bar{x}_0 = x_0/s$.

The left-hand side in Eq. (8) is the residual flow velocity at $Z=Z_i$, in the absence of the effect of the vortex singularity situated there. The right-hand side derives from an approximation to the true vector sum of these forces, which is

$$ip\,U\left\{\frac{d\Gamma_i}{dx}(Z_i\mp s) + \Gamma_i\frac{dZ_i}{dx}\right]$$
$$+ i\Gamma_i\epsilon\bar{p}[\bar{Z}_i + i\alpha(\bar{x}_{00}-\bar{x}_0)]\}, \quad i=1,2$$

This approximation is legitimate if 1) $(dZ_i/dx)\approx(Z_i/s)\epsilon$, i.e., if one assumes that the concentrated vortex lines lie "close" to the wing leading edges; 2) $(d\Gamma_i/dx)\cdot(Z_i\mp s) \approx n_i\Gamma_i\cdot\epsilon(Z_i\mp s)/s$, i.e., if one assumes that the concentrated vortex strengths vary locally as

$$\Gamma_i = \text{const.}\quad x^{n_i} \tag{9}$$

i.e.,

$$\frac{d\Gamma_i}{dx} = \frac{n_i\Gamma_i}{x} \tag{10}$$

Both these assumptions are justified exactly for the case of a wing at angle of attack and zero roll, if $n_i = 1$, since the flow is conical. At the other extreme, for the case of a wing in pure roll at zero angle of attack, the assumptions were tested against the known part-numerical solution of Hanin and Mishne[8] by comparing the value of $\Gamma_0 = \Gamma_1 = \Gamma_2$, derived, for pure roll by the present method, using $n_1 = 2$, with that obtained in that source. The agreement was found to be excellent.

For intermediate cases, such as the ones under investigation with mixed angle-of-attack $\bar{\alpha}$ and roll $\bar{p}$, we shall assume simply that

$$n_1 = n_2 = \frac{|\bar{p}| + |\bar{\alpha}|}{|\bar{p}/2| + |\bar{\alpha}|} = n \tag{11}$$

which satisfy the boundary values of n (i.e., for pure roll, $\bar{\alpha} = 0$ and for pure angle of attack, $\bar{p} = 0$) and give convenient interpolative values for n for mixed flows. The authors were further helped in making this assumption by the relative insensitiveness of the solutions to the actual value of n.

We can now proceed to derive another four relations relating the six unknowns $(\rho_1, \bar{\Gamma}_i, \beta_1)$ and $(\rho_2, \bar{\Gamma}_2, \beta_2)$. Taking the conjugate of Eq. (8) gives

$$(v_i - iw_i)_- = \epsilon U\{(n_i + 1)\bar{\bar{Z}}_i \mp n_i - i\bar{p}[\bar{\bar{Z}}_i - i\bar{\alpha}(\bar{s}_0 - 1)]\} \tag{12}$$

where

$$(v_i - iw_i)_- = \left\{\frac{d}{dZ}\left[W(\xi) - \frac{i\Gamma_i}{2\pi}\ln(Z - Z_i)\right]\right\}_{Z - Z_i} \quad i = 1,2 \tag{13}$$

In Eq. (13), $W(\xi)$ is given by Eq. (5) and W_1 and W_2 by Eqs. (1) and (4), respectively. Performing the operations involved in Eq. (13), obtains, after some arithmetic

$$\frac{1}{\epsilon U}(v_1 - iw_1)_- = \frac{i\bar{p}}{\bar{\xi}_2(\bar{\xi}_2^2 - 1)} - \frac{i\bar{\alpha}(\bar{\xi}_2^2 + 1)}{(\bar{\xi}_2^2 - 1)} + \frac{2i\bar{\xi}_2^2}{(\bar{\xi}_2^2 - 1)}$$

$$\left\{\frac{-\bar{p}^2\bar{\Gamma}_1}{(\bar{p}_1^2 - 1)\bar{\xi}_1} - \frac{\bar{\Gamma}_1}{\bar{\xi}_1(\bar{\xi}_1^2 - 1)} + \frac{\bar{\Gamma}_2\bar{\xi}_2(\bar{p}_2^2 - 1)}{(\bar{\xi}_1 - \bar{\xi}_2)(\bar{p}_2^2\bar{\xi}_1 - \bar{\xi}_2)}\right\} \tag{14}$$

with a similar expression for $(v_2 - iw_2)_-$.

On making use of Eq. (12), for $i = 1,2$, one finally obtains the two complex expressions

$$i(\overline{n+1}\bar{\bar{Z}}_1 - n) + + \bar{p}(\bar{\bar{Z}}_1 - i\bar{\alpha}(\bar{s}_0 - 1)) = \frac{-\bar{p}}{\bar{\xi}_1(\bar{\xi}_1^2 - 1)}$$

$$+ \frac{\bar{\alpha}(\bar{\xi}_1^2 + 1)}{(\bar{\xi}_1^2 - 1)} - \frac{2\bar{\xi}_1^2}{(\bar{\xi}_1^2 - 1)}\left\{\frac{-\bar{p}_1^2\bar{\Gamma}_1}{(\bar{p}_1^2 - 1)\bar{\xi}_1}\right.$$

$$\left. - \frac{\bar{\Gamma}_1}{\bar{\xi}_1(\bar{\xi}_1^2 - 1)} + \frac{\bar{\Gamma}_2\bar{\xi}_2(\bar{p}_2^2 - 1)}{(\bar{\xi}_1 - \bar{\xi}_2)(\bar{p}_2^2\bar{\xi}_1 - \bar{\xi}_2)}\right\} \tag{15a}$$

$$i(\overline{n+1}\bar{\bar{Z}}_2 + n) + \bar{p}(\bar{\bar{Z}}_2 - i\bar{\alpha}(\bar{s}_0 - 1)) = \frac{-\bar{p}}{\bar{\xi}_2(\bar{\xi}_2^2 - 1)}$$

$$+ \frac{\bar{\alpha}(\bar{\xi}_2^2 + 1)}{(\bar{\xi}_2^2 - 1)} - \frac{2\bar{\xi}_2^2}{(\bar{\xi}_2^2 - 1)}\left\{\frac{-\bar{p}_2^2\bar{\Gamma}_2}{(\bar{p}_2^2 - 1)\bar{\xi}_2}\right.$$

$$\left. - \frac{\bar{\Gamma}_2}{\bar{\xi}_2(\bar{\xi}_2^2 - 1)} + \frac{\bar{\Gamma}_1\bar{\xi}_1(\bar{p}_1^2 - 1)}{(\bar{\xi}_2 - \bar{\xi}_1)(\bar{p}_1^2\bar{\xi}_2 - \bar{\xi}_1)}\right\} \tag{15b}$$

for the determination of $\bar{Z}_1, \bar{Z}_2, \bar{\Gamma}_1$ and $\bar{\Gamma}_2$. Thus the two Eqs. (7)and the preceding two complex equations enable the six quantities $\bar{x}_1, \bar{y}_1, \bar{x}_2, \bar{\Gamma}_1, \bar{\Gamma}_2$, i.e., the positions and strengths of the two concentrated vortices off "leading" and "trailing" edges, to be found. The equations are a set of nonlinear simultaneous algebraic equations which can be solved by a variant of the optimum descent technique. This has been done in representative ranges of the controlling parameters $\bar{s}_0$, $\bar{\alpha}$, and $\bar{p}$, and the results tabulated in Table 1. Figures 4 and 5 give a visual display of some of these results and show the coordinate positions of the concentrated normalized with respect to the local semispan, vortices, for two values of $\bar{s}_0$, the parameter introducing the chordwise position of the axis of roll, and two of the incidence for a set of values of $\bar{p}$. The case illustrated in Fig. 4 allows also the projection of the positions of the concentrated vortices in the crossflow planes on a plane normal to the wing surface.

III. Pressure Distribution Along a Span

For the case considered, for the body axes adopted, and on the surface of the rotating wing, the pressure coefficient is given by

$$C_p = -\frac{2u}{U} - \frac{(v^2 - w^2)}{U^2} + \alpha^2 \tag{16}$$

with

$$u = \frac{\partial\phi}{\partial x}, \quad v = \frac{\partial\phi}{\partial y}, \quad w = \frac{\partial\phi}{\partial z} \tag{17}$$

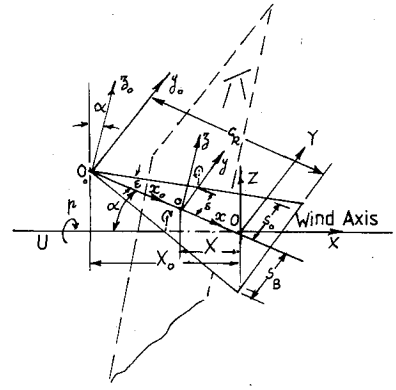

Fig. 1 Delta wing in roll at incidence; geometry.

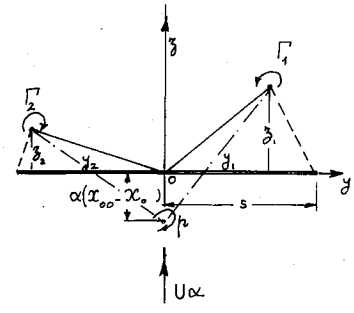

Fig. 2 Cross-flow plane, Z-plane.

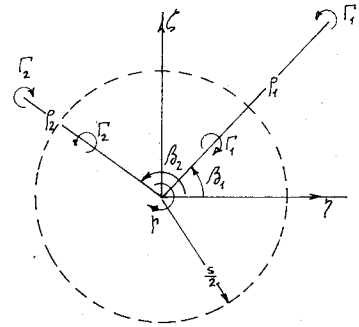

Fig. 3 Transformed plane, ξ-plane. $\xi = Z + (Z^2 - 1)^{1/2}$.

In Eqs. (17), ϕ is the real part of $W(Z)$ on the surface of the wing.

Using Eqs. (5), (1), and (4) in the evaluation of the derivatives in Eqs. (17) leads, after substitution in Eq. (16), to the expression for C_p

$$\frac{C_p}{\epsilon^2} = 2\{\frac{\bar{p}}{2} - \bar{\alpha}\sec\theta - \frac{\bar{\Gamma}_1(\bar{\rho}_1^2-1)}{1+\bar{\rho}_1^2-2\bar{\rho}_1\cos(\theta-\beta_1)} - \frac{\bar{\Gamma}_2(\bar{\rho}_2^2-1)}{1+\bar{\rho}_2^2-2\bar{\rho}_2\cos(\theta-\beta_2)}\}\cot\theta$$

$$+2(\bar{\Gamma}_1+\bar{p}\cdot\frac{\partial\bar{\Gamma}_1}{\partial\bar{p}})\tan^{-1}[\frac{(\bar{\rho}_1-[1/\bar{\rho}_1])\sin(\theta-\beta_1)}{2-(\bar{\rho}_1+[1/\bar{\rho}_1])\cos(\theta-\beta_1)}]+2(\bar{\Gamma}_2+\bar{p}\cdot\frac{\partial\bar{\Gamma}_2}{\partial\bar{p}})\tan^{-1}[\frac{(\bar{\rho}_2-[1/\bar{\rho}_2])\sin(\theta-\beta_2)}{2-(\bar{\rho}_2+[1/\bar{\rho}_2])\cos(\theta-\beta_2)}]$$

$$+4\bar{\Gamma}_1\bar{p}\frac{\sin(\theta-\beta_1)}{1+\bar{\rho}_1^2-2\bar{\rho}_1\cos(\theta-\beta_1)}\cdot\frac{\partial\bar{\rho}_1}{\partial\bar{p}}+4\bar{\Gamma}_2\bar{p}\frac{\sin(\theta-\beta_2)}{1+\bar{\rho}_2^2-2\bar{\rho}_2\cos(\theta-\beta_2)}\cdot\frac{\partial\bar{\rho}_2}{\partial\bar{p}}$$

$$+2\bar{\Gamma}_1\bar{p}\frac{(\bar{\rho}_1^2-1)}{1+\bar{\rho}_1^2-2\bar{\rho}_1\cos(\theta-\beta_1)}\cdot\frac{\partial\beta_1}{\partial\bar{p}}+2\bar{\Gamma}_2\bar{p}\frac{(\bar{\rho}_2^2-1)}{1+\bar{\rho}_2^2-2\bar{\rho}_2\cos(\theta-\beta_2)}\cdot\frac{\partial\beta_2}{\partial\bar{p}}$$

$$-[\{\bar{\alpha}[\cos\theta-\bar{p}(\bar{s}_0-1)\sin\theta]+\frac{\bar{\Gamma}_1(\bar{\rho}_1^2-1)}{1+\bar{\rho}_1^2-2\bar{\rho}_1\cos(\theta-\beta_1)}+\frac{\bar{\Gamma}_2(\bar{\rho}_2^2-1)}{1+\bar{\rho}_2^2-2\bar{\rho}^2\cos(\theta-\beta_2)}-\frac{\bar{p}\cos2\theta}{2}\}^2$$

$$-\frac{p^2\sin^2 2\theta}{4}]\operatorname{cosec}^2\theta+\bar{\alpha}^2\bar{p}^2(\bar{s}_0-1)^2+\bar{\alpha}^2 \tag{18}$$

In Eq. (18) all the quantities involved are known at each crossflow section of the wing (see Table 1), and the derivatives $\partial\bar{\rho}_i/\partial\bar{p}$ and $\partial\beta_i/\partial\bar{p}$ are evaluated from the tabulated value of $\bar{\rho}_i$ and β_i. Figure 6 shows the pressure distribution C_p/ϵ^2 over a delta wing at $\bar{p}=0.883$ rolling, at zero incidence and the result is compared with that obtained by Hanin and Mishne.[8] The present results give somewhat different values of the position of the concentrated vortices and rather better agreement with observed experimental measurements.[12]

IV. Forces and Moments Acting on the Wing

For a slender wing in the type of motion considered in this paper, the relevant aerodynamic forces acting on it are the lift L and the lift-induced drag, D_i, which is derived simply from

$$D_i = L.\alpha \tag{19}$$

The aerodynamic moments similarly reduce to two components whose values will depend on the position of the roll axis, namely the rolling moment due to roll in separated flow and at incidence $\mathfrak{L}$, and the pitching moment due to that roll, $\mathfrak{M}$. It is clear that this pitching moment is a coupling effect which derived its action from the fact that the roll takes place at incidence and, hence, creates a pitching inbalance additional to any due to the angle of attack. Thus, for a true delta wing whose axis of roll passes through its center of area, the pitching moment is different from zero, and represents a pure roll-pitch coupling action.

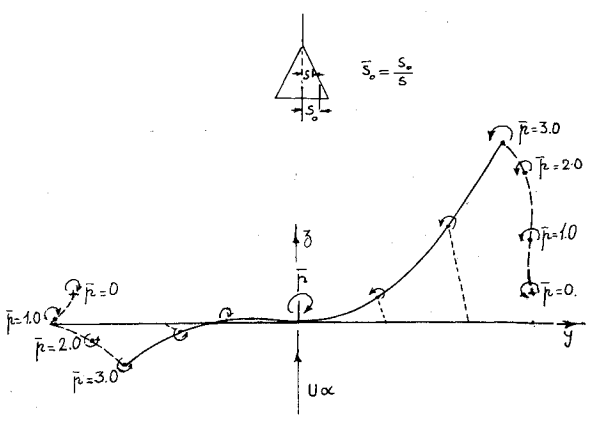

Fig. 4 Vortex location:

A. Lift of a Slender Wing in Roll and at Incidence

L is calculated most simply by overall momentum flux considerations at the boundaries of a large control cylinder, whose axis coincides with OX and one of whose ends is the Trefftz-plane. It can be shown that the value of L is determined, at any angle of attack α, solely by the strengths and positions of the isolated vortices (now known) in the crossflow plane parallel to the Trefftz-plane and touching the wing trailing edge, assumed straight and normal to the direction of

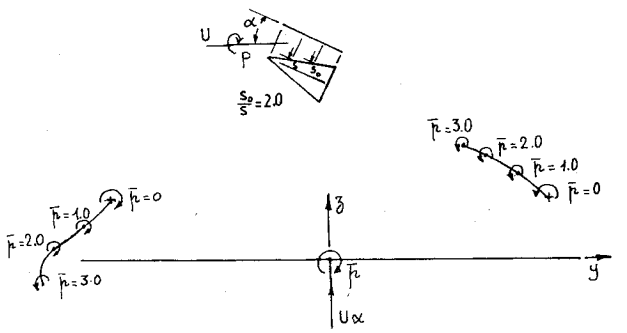

Fig. 5 Vortex location: $\bar{s}_0=2.0$, $\bar{\alpha}=1.0$.

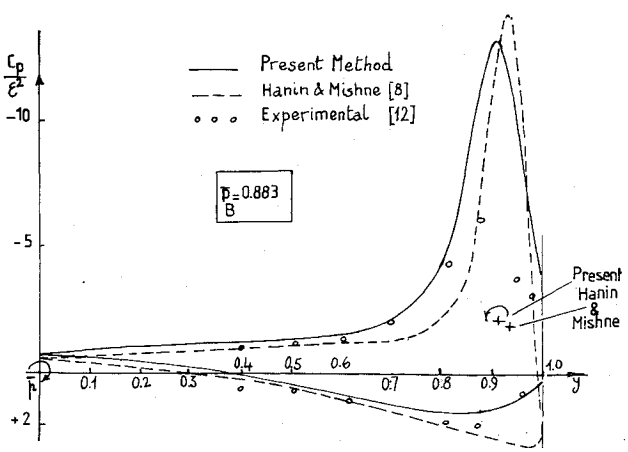

Fig. 6 Trailing edge pressure distribution for rolling delta wing. $\bar{\alpha}=0$.

Table 1a $\bar{\alpha}=0.5$

$\bar{p}$	$\bar{s}_0$	$\bar{\Gamma}_1$	$\bar{\Gamma}_2$	y_1	z_1	y_2	z_2
	0	−0.412	0.239	0.897	0.173	−0.929	0.071
	0.5	−0.423	0.234	0.891	0.168	−0.931	0.072
0.3	1	−0.433	0.228	0.887	0.164	−0.932	0.074
	2	−0.545	0.216	0.880	0.155	−0.936	0.078
	4	−0.494	0.191	0.869	0.142	−0.945	0.087
	0	−0.496	0.158	0.898	0.238	−0.951	0.041
	0.5	−0.518	0.151	0.884	0.225	−0.953	0.042
0.6	1	−0.542	0.144	0.873	0.213	−0.954	0.044
	2	−0.589	0.128	0.855	0.194	−0.958	0.048
	4	−0.680	0.092	0.835	0.165	−0.980	0.064
	0	−0.635	0.078	0.907	0.340	−0.974	+0.018
	0.5	−0.671	0.070	0.876	0.311	−0.975	+0.018
1.0	1	−0.711	0.063	0.852	0.286	−0.976	+0.019
	2	−0.798	0.050	0.820	0.247	−0.980	+0.022
	4	−0.983	0.057	0.787	0.198	−1.158	−0.165
	0	−0.853	0.016	0.907	0.470	−0.993	0.003
	0.5	−0.900	0.010	0.858	0.420	−0.994	0.003
1.5	1	−0.959	0.006	0.821	0.377	−0.996	0.002
	2	−1.098	0.002	0.772	0.310	−0.998	0.002
	0	−1.104	−0.093	0.887	0.589	−0.827	−0.051
	0.5	−1.158	−0.093	0.828	0.519	−0.830	−0.0852
2.0	1	−1.232	−0.079	0.781	0.458	−0.841	−0.134
	2	−1.418	−0.066	0.721	0.365	−0.934	−0.309
	0	−1.640	−0.318	0.806	0.770	−0.704	−0.158
	0.5	−1.712	−0.292	0.740	0.669	−0.718	−0.224
3.0	1	−1.814	−0.267	0.689	0.581	−0.748	−0.312

Table 1b $\bar{\alpha}=1$

$\bar{p}$	$\bar{s}_0$	$\bar{\Gamma}_1$	$\bar{\Gamma}_2$	y_1	z_1	y_2	z_2
	0	−0.825	0.726	0.890	0.323	−0.877	0.168
	0.5	−0.853	0.699	0.871	0.309	−0.884	0.173
	1	−0.891	0.671	0.856	0.295	−0.891	0.179
0.3	1.5	−0.925	0.634	0.843	0.283	−0.900	0.186
	2	−0.959	0.615	0.832	0.272	−0.910	0.194
	4	−1.095	0.499	0.800	0.239	−0.991	0.235
	0	−0.891	0.665	0.931	0.425	−0.892	0.123
	0.5	−0.947	0.618	0.880	0.387	−0.900	0.129
0.6	1	−1.011	0.572	0.843	0.354	−0.909	0.137
	1.5	−1.079	0.525	0.815	0.326	−0.923	0.146
	2	−1.149	0.475	0.794	0.303	−0.942	0.159
	4	−1.476	0.387	0.745	0.247	−1.334	0.105
	0	−1.041	0.599	0.983	0.574	−0.911	0.087
	0.5	−1.107	0.532	0.887	0.498	−0.918	0.091
1.0	1	−1.203	0.462	0.819	0.433	−0.928	0.098
	1.5	−1.317	0.406	0.774	0.382	−0.944	0.109
	2	−1.439	0.334	0.743	0.342	−0.977	0.124
	4	−2.105	0.497	0.683	0.264	−1.697	−0.314
	0	−1.287	0.536	1.010	0.754	−0.928	0.062
	0.5	−1.357	0.450	0.875	0.629	−0.936	0.064
1.5	1	−1.484	0.375	0.779	0.524	−0.946	0.068
	1.5	−1.654	0.301	0.717	0.443	−0.961	0.078
	2	−1.846	0.201	0.678	0.384	−1.033	0.090
	0	−1.560	0.487	0.994	0.090	−0.941	0.047
	0.5	−1.637	0.389	0.841	0.740	−0.949	0.047
2.0	1	−1.797	0.307	0.731	0.599	−0.958	0.050
	1.5	−2.023	0.229	0.661	0.492	−0.973	0.058
	0	−2.133	0.415	0.901	1.132	−0.958	0.030
3.0	0.5	−2.245	0.307	0.744	0.897	−0.965	0.029
	1	−2.478	0.220	0.629	0.702	−0.972	0.030

Table 1c $\bar{\alpha}=2$

$\bar{p}$	$\bar{s}_0$	$\bar{\Gamma}_1$	$\bar{\Gamma}_2$	y_1	z_1	y_2	z_2
	0	−1.867	2.063	0.949	0.587	−0.812	0.329
	0.5	−1.947	1.946	0.887	0.547	−0.834	0.340
0.3	1	−2.042	1.835	0.838	0.512	−0.859	0.354
	2	−2.260	1.627	0.769	0.459	−0.934	0.395
	4	−2.840	1.433	0.681	0.409	−1.352	0.475
	0	−1.938	2.204	1.090	0.778	−0.805	0.270
	0.5	−2.024	1.968	0.932	0.679	−0.833	0.278
0.6	1	−2.178	1.753	0.821	0.592	−0.869	0.294
	2	−2.618	1.359	0.695	0.482	−1.037	0.361
	4	−4.126	1.761	0.578	0.408	−2.148	0.096
	0	−2.159	2.373	1.236	1.038	−0.809	0.215
	0.5	−2.220	2.000	0.964	0.854	−0.840	0.223
1.0	1	−2.408	1.671	0.784	0.690	−0.881	0.236
	2	−3.205	1.135	0.600	0.512	−1.298	0.253
	4	−5.932	2.299	0.492	0.403	−2.870	−0.621
	0	−2.468	2.514	1.301	1.346	−0.821	0.177
	0.5	−2.467	2.022	0.960	1.044	−0.854	0.178
1.5	1	−2.741	1.592	0.720	0.785	−0.895	0.187
	2	−4.172	1.373	0.508	0.534	−1.582	−0.195
	0	−2.767	2.588	1.283	1.591	−0.835	0.148
	0.5	−2.799	2.021	0.913	1.190	−0.867	0.148
2.0	1	−3,100	1.527	0.650	0.851	−0.906	0.154
	2	−5.226	1.748	0.445	0.541	−1.616	−0.591
	0	−3.334	2.619	1.149	1.914	−0.861	0.110
3.0	0.5	−3.409	1.979	0.782	1.368	−0.889	0.109
	1	−3.854	1.420	0.523	0.920	−0.924	0.112

the stream. This yields

$$L=qS\cdot\frac{\pi}{2}\overline{AR}\,\alpha\left[1-\left\{\frac{\bar{\Gamma}_1}{\bar{\alpha}}\left(\bar{\rho}_1-\frac{1}{\bar{\rho}_1}\right)\cos\beta_1+\frac{\bar{\Gamma}_2}{\bar{\alpha}}\left(\bar{\rho}_2-\frac{1}{\bar{\rho}_2}\right)\cos\beta_2\right\}\right]_B \tag{20}$$

In nondimensional form with $C_L=L/qS$

$$C_L=\frac{\pi}{2}\overline{AR}\,\alpha\left[1-\left\{\frac{\bar{\Gamma}_1}{\bar{\alpha}}\left(\bar{\rho}_1-\frac{1}{\bar{\rho}_1}\right)\cos\beta_1+\frac{\bar{\Gamma}_2}{\bar{\alpha}}\left(\bar{\rho}_2-\frac{1}{\bar{\rho}_2}\right)\cos\beta_2\right\}\right]_B \tag{21}$$

where the suffix "B" denotes conditions at the wing trailing edge. This result for C_L reduces, of course, to the known Brown and Michael result, for the case of no roll

$$C_L = \frac{\pi}{2}\overline{AR}\,\alpha\left[1+\frac{4\bar{\Gamma}_0}{\bar{\alpha}}R\{(Z^2-1)^{1/2}\}\right]_B \tag{22}$$

The lift-induced drag, for the general case, is obtained from Eqs. (19) and (20). In Eqs. (20-22) $\overline{AR}$, is the aspect ratio $(4s_B^2/S)$.

B. Rolling Moment of a Slender Wing at Incidence in Detached Flow

The axis of the roll is the wind axis. From overall moment of momentum considerations involving a large control surface identical to that used in the calculations of the lift, it can be shown[2] that the rolling moment acting on the configuration in roll and angle of attack in the detached regime is

$$C_\ell = \frac{\pi}{32}\overline{AR}\,\epsilon\left[\bar{p}+2\bar{\Gamma}_1\{4|\bar{Z}_1|^2-(\frac{1}{\bar{\xi}_1^2}+\frac{1}{\bar{\xi}_1^2}+2)\}\right.$$

$$\left.+2\bar{\Gamma}_2\{4|\bar{Z}_2|^2-(\frac{1}{\bar{\xi}_2^2}+\frac{1}{\bar{\xi}_2^2}+2)\}\right]_B \tag{23}$$

where, once more, the first term in the brackets on the right-hand side represents the linear contribution to C_ℓ in undetached flow due to $\bar{p}$, and the other two terms in that bracket represent the nonlinear contributions due to vortex separation at the wing leading edges. In Eq. (23), C_ℓ is defined by $C_\ell = (\mathcal{L}/2qSs_B)$.

In the previous expression $(\bar{\xi}_1,\bar{\Gamma}_1)_B$ and $(\bar{\xi}_2,\bar{\Gamma}_2)_B$ can be obtained for any flight condition described by the set $(\bar{s}_{0B},\bar{\alpha},\bar{p}_B)$ from Table 1 and Eq. (2). C_ℓ is nonlinear in $\bar{p}_B$, and the value of the derivative at $\bar{p}_B=\bar{p}_{B1}$, i.e., $(\partial C_\ell/\partial\bar{\Gamma}_B)\bar{p}_B=\bar{p}_{B1}$, will obviously depend on the operating point $\bar{p}_{B1}$ at which it is desired to assess it. An example of this assessment will be considered in the next section.

C. Pitching Moment Coupling Caused by Roll of a Slender Wing at Incidence in Detached Flow

Once again a control volume method similar to that used previously in the assessment of the lift and rolling moment, yields, from a consideration of the appropriate component of the moment of momentum across its surface, the following expression for $\mathfrak{M}$, the pitching moment:

$$\mathfrak{M} = -Lc_R\left[(1-\bar{s}_{0B})-\frac{\mathfrak{I}\{\int_0^1 \bar{a}_1 d\bar{x}\}}{\mathfrak{I}\{\bar{a}_1\}_B}\right] \tag{24}$$

where c_R is the root chord of the wing and x is normalized with respect to it, i.e., $\bar{x}=(x/c_R)$. In Eq. (24), $\mathfrak{I}\{\ \}$ is the imaginary part of $\{\ \}$, and $\bar{a}_1$ will, generally, be complex and represent the coefficient of $1/Z$ in the expansion of $W(Z)$ in powers of $1/Z$. It can be shown that

$$\mathfrak{I}\{\bar{a}_1\} = s^2\left[1-\{\frac{\bar{\Gamma}_1}{\bar{\alpha}}(\bar{p}_1-\frac{1}{\bar{p}_1})\cos\beta_1+\frac{\bar{\Gamma}_2}{\bar{\alpha}}(\bar{p}_2-\frac{1}{\bar{p}_2})\cos\beta_2\right]$$

Hence, Eq. (24) becomes, on substitution for $\mathfrak{I}$, therein:

$$C_m = -C_L\left[(1-\bar{s}_{0B})-\frac{\int_0^1\left[1-\{\frac{\bar{\Gamma}_1}{\bar{\alpha}}(\bar{p}_1-\frac{1}{\bar{p}_1})\cos\beta_1+\frac{\bar{\Gamma}_2}{\bar{\alpha}}(\bar{p}_2-\frac{1}{\bar{p}_2})\cos\beta_2\}\right]\bar{s}^2 d\bar{x}}{\left[1-\{\frac{\bar{\Gamma}_1}{\bar{\alpha}}(\bar{p}_1-\frac{1}{\bar{p}_1})\cos\beta_1+\frac{\bar{\Gamma}_2}{\bar{\alpha}}(\bar{p}_2-\frac{1}{\bar{p}_2})\cos\beta_2\}\right]_B}\right] \tag{25}$$

where $\bar{s}=s/s_B$, with C_m defined as: $C_m=\mathfrak{M}/qSc_R$.

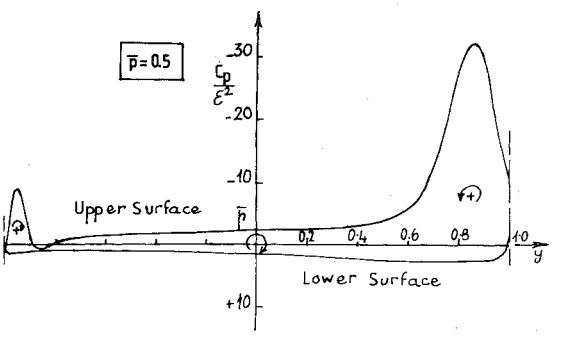

Fig. 7 Sectional spanwise pressure distribution for rolling delta wing; $\bar{s}_0=2$, $\bar{\alpha}=0.5$.

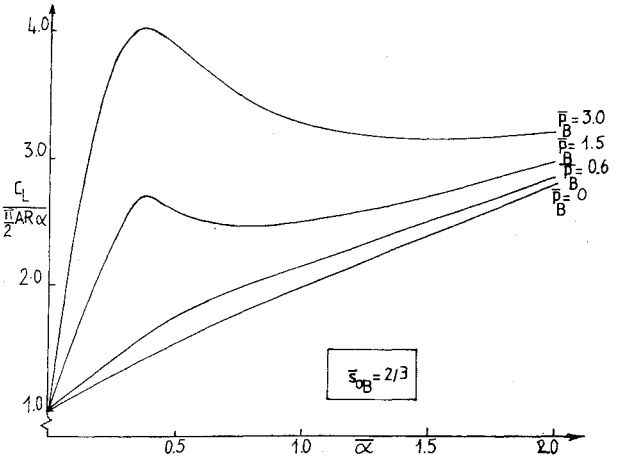

Fig. 8 Lift coefficient curve for rolling delta wing.

Equation (25) gives the value of the roll-induced pitching moment coefficient C_m and the value of the roll-induced pitching moment coefficient C_m and the value of the derivative $(\partial C_m/\partial\bar{p})$ will, once more depend on the operating point, $\bar{p}_B=\bar{p}_{B1}$, in the given flight condition defined by the set $(\bar{\alpha},\bar{s}_{0B})$, at which its assessment is required. A very few sections, chordwise, will suffice to give a reliable value for the integral on the right-hand side of Eq. (25), the function C_m being well-behaved. One such set of operations is described and performed in the next section.

V. Example

The basic example used to illustrate the preceding results is provided by a true delta wing operating at various $\bar{\alpha}$'s and whose rolling axis crosses the wing at $\bar{x}=\frac{2}{3}$, $(\bar{s}_{OB}=\frac{2}{3})$. It is required to determine: a) the spanwise load distributions at $\bar{\alpha}=0.5$, at the chordwise station, $\bar{s}_0=2.0$ (i.e., at $\bar{x}=\frac{1}{3}$), for $\bar{p}_0=1$; b) the lift coefficient as function of $\bar{\alpha}$, for $\bar{p}_B=0.6,15,3$; and c) the rolling and pitching moment coefficients due to roll as functions of $\bar{p}_B$, for $\bar{\alpha}=0.5$, 1,2.

a) The spanwise pressure distribution required at $\bar{x}=\frac{1}{3}$ is shown in Fig. 7. There is a marked relative moment of the "downgoing" vortex inwards and away from the wing, with increased vortex strength and a concurrently marked relative movement of the "upgoing" vortex outwards and towards the wing, with a correspondingly decreased vortex strength. These movements are accompanied by the creation of the unsymmetrically placed and unequal peaks shown in the figure.

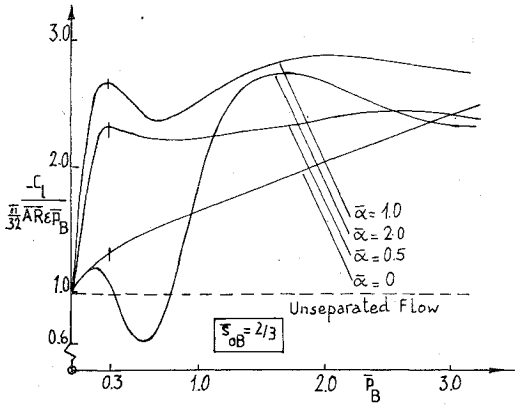

Fig. 9 Damping-in-roll coefficient's dependence on $\bar{p}_B$.

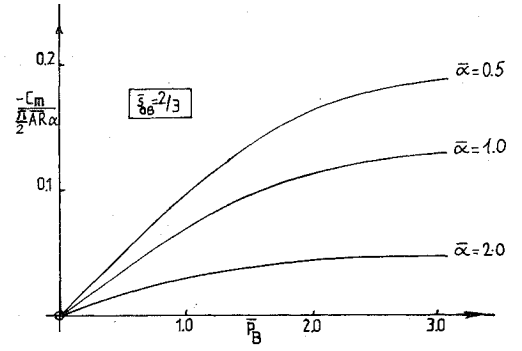

Fig. 10 Pitch-roll coupling coefficient's dependence on $\bar{p}_B$.

b) Figure 8 shows the C_L [or (C_{D_i}/α)] dependence on $\bar{\alpha}$, for $\bar{p}_B = 0.6, 1.5$, and 3. For comparative purposes the $C_L(\bar{\alpha})$ dependence for no roll (Brown and Michael's result) is also shown. It is seen that for small rates of roll $\bar{p}_B < 0.5$, say, this relationship is not much affected. As the rate of roll increases, however, beyond that value, the $C_L(\bar{\alpha})$ curve begins to show a characteristic hump at about $\bar{\alpha} = 0.4$, which becomes more pronounced as $\bar{p}_B$ increases. As $\bar{\alpha}$ increases beyond 0.4, the curve slumps down and approaches the chracteristic $C_L(\bar{\alpha})$ curve for no roll, asymptotically from above. Quantitatively the effect of the rolling wing on the lift curve slope at incidence and in separated flow can be quite impressive, reaching at $\bar{p}_B = 1.5$ a maximum of some twice its value in the absence of roll at moderate incidences ($\bar{\alpha} \leq 0.5$).

c) Figures 9 and 10 show the dependence of C_ℓ and C_m for that wing on the rate of the roll $\bar{p}_B$ for the set of values of $\bar{\alpha} = 0.5$, 1, 2. On the same figures the curves for $\alpha = 0$ are also shown to illustrate the way in which the presence of incidence affects radically the theoretical damping-in-roll of a delta wing in separated flow.

Thus, in Fig. 9, the function $(-C_\ell/(\pi/32)\epsilon\overline{AR}\bar{p}_B)$ is plotted against $\bar{p}_B$. For $\bar{\alpha} = 0.5$ and for $\bar{\alpha} = 1.0$ there is once again a rapid increase in the value of that function with an overshoot apparent, especially in the latter case with both appearing to tend in oscillatory fashion and asymptotically to the smooth curve for that function in the absence of incidence, as $\bar{p}_B \to \infty$. For $\bar{\alpha} = 2$, however, the behavior of the function is more extreme, barely rising above its *linear* value of unity for $\bar{p}_B < 0.3$, dipping markedly below that, at about $\bar{p}_B = 0.6$, to a value of just over 0.6 and then rising rapidly overshooting above the curve for the zero-incidence wing and henceforth exhibiting the low-amplitude oscillatory character of the previous two curves. These latter conclusions may not be significant however, due to the possible failure of the basic assumptions at those high incidences. Thus, whereas the nonlifting wing in separated flow will possess a theoretical value of the damping-in-roll derivative $[(-\partial C_L/\partial p_B)/(\pi/32)\overline{AR}\epsilon]_{pB=0} = 1.15$ at $\bar{\alpha} = 0$, the same derivative becomes approximately 1.65 at $\bar{\alpha} = 0.5$ and 2.05 at $\bar{\alpha} = 1$. Thus a slender wing at high, but not excessively high angle of attack $0 < \bar{\alpha} < 1$, such as at landing and take-off will tend to be more stable in roll than the same wing at very low angles of attack. Figure 11 shows a comparison of the value of the derivative $(-\partial C_\ell/\epsilon\,\partial\bar{p}_B)_{pB=\bar{p}Bl}$ at different angles of attack in separated flow for a particular model as obtained by three methods: a) Boyden's[10] method using Polhamus' leading edge suction analogy; b) experimentally, as presented in Ref. 11, and used in Ref. 10; and c) that method developed in this paper, for the value of $\bar{p}_{Bl} = 0.3$, which is the operating value for the case under test. The agreement between (b) and (c) is remarkable, and the basic behavior of the derivative at different angles of attack is clearly reproduced by the theoretical model. In (c)the results were derived for the closest equivalent true delta wing to the experimental model, with a semiapex angle of $\epsilon = 15°$.

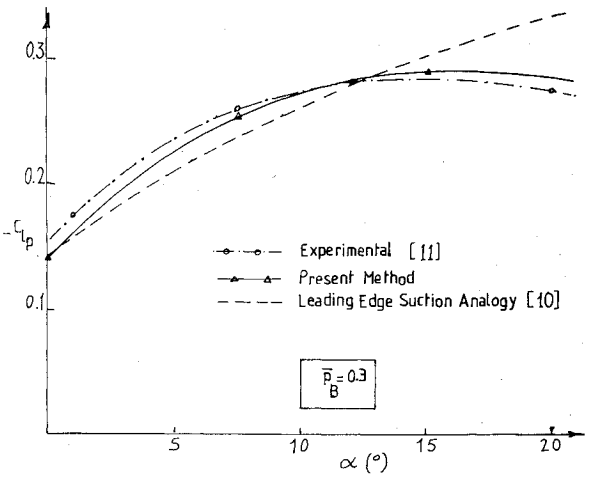

Fig. 11 Comparison of experimental data with theory.

In Fig. 10, the function $-C_m/(\pi/2)\overline{AR}\alpha$ is plotted against $\bar{p}_B$ and shows that the pitching moment due to roll-coupling developed is most significant at relatively low angles of attack and at low rates of roll. This roll-pitch coupling effect always leads to a nose-down pitching moment, the value of the derivative $([-\partial C_m/\partial\bar{p}_B]/(\pi/2)\overline{AR}\alpha)_{pB=0}$ reaching 0.1, at $\bar{\alpha} = 0.5$. In other words there is a tendency to a rapid movement backwards of the effective center of normal force on the wing, at low rates of roll, this effect being most severe at low or moderate angles of attack.

Conclusions

The main points deriving from the preceding simplified analysis of a slender wing in separated flow rolling at angle of attack about its wind axis are as follows: a) There is an increase in the lift experienced by the wing at any angle of attack due to the rolling action compared to that for the same wing at the same angle of attack but with no roll. This increase becomes more important as the rate of roll increases. b) There is a marked relative increase in the (damping) rolling moment experienced by the wing at any given angle of attack, an effect which is especially pronounced at low rates of roll and low-to-medium angles of attack. c) There is present a nose-down pitching moment due to pitch-roll coupling, for a slender wing in separated flow rolling at angle of attack which may lead to a significant coupling of the lateral and longitudinal responses of the wing-craft system to lateral control movement.

References

[1] Lamb, H., *Hydrodynamics*, 6th ed., Cambridge University Press, Cambridge, England, 1932, pp.86-90.

[2] Nielson, J., *Missile Aerodynamics*, McGraw Hill, New York, 1960, pp. 101-106.

[3]Bryson, A. E., Jr., "Evaluation of the Inertia Coefficients of the Cross-Sections of Slender Bodies," *Journal of the Aeronautical Sciences*, Vol. 21, Jan. 1954, p. 59.

[4]Sacks, A. H., "Aerodynamic Forces, Moments and Stability Derivatives for Slender Bodies of General Cross-Sections," NACA TN 3283 (1954).

[5]Lomax, H. and Heaslet, M. A., "Damping-In Roll Calculations for Slender Swept-Back Wings and Slender Wing-Body Combinations," NACA TN 1950, 1949.

[6]Nonweiler, T., "Theoretical Stability Derivatives of a Highly Swept Delta-Wing and Slender Body Combination," College of Aeronautics, Cranfield, Eng., Rept. 50, 1961.

[7]Brown, C.E. and Michael, W.H., "Effect of Leading Edge Separation on the Lift of a Delta Wing," NACA TN 3430, 1955.

[8]Hanin, M. and Mishne, D., "Flow about a Rolling Slender Wing with Leading Edge Separation," *Israel Journal of Technology*, Vol. 11, June 1973, pp. 131-136.

[9]Polhamus, E. C., "Predictions of Vortex Lift Characteristics Based on Leading-Edge Suction Analogy," *Journal of Aircraft*, Vol. 8, April 1971, pp. 193-199.

[10]Boyden, R. P., "Effects of Leading-Edge Vortex Flow on the Roll Damping of Slender Wings," *Journal of Aircraft*, Vol. 8, July 1971, pp. 543-547.

[11]Henderson, W. P., Phillips, W. P., and Gainer, T. G., "Rolling Stability Derivatives of a Variable-Sweep Tactical Fighter Model at Subsonic and Transonic Speeds," NASA TN D3845, 1967.

[12]Harvey, J. K., "A Study of the Flow Field Associated with a Steadily Rolling Slender Delta Wing," *Journal of the Royal Aeronautical Society*, Vol. 68, Feb. 1964, pp. 106-110.